

Origin and Activity of Oxidized Gold in Water-Gas-Shift Catalysis

Zhi-Pan Liu, Stephen J. Jenkins, and David A. King

Department of Chemistry, University of Cambridge, Lensfield Road, Cambridge CB2 1EW, United Kingdom

(Received 26 January 2005; published 19 May 2005)

As a promising route for large-scale H₂ production, the water-gas-shift reaction (WGS, CO + H₂O → CO₂ + H₂) on ceria-supported Au catalysts is of enormous potential in efforts to move towards a hydrogen economy. Recent research suggests that this reaction is in fact catalyzed by Au cations instead of the conventionally regarded metallic Au particles. Here density functional theory calculations demonstrate that the presence of empty localized nonbonding *f* states in CeO₂ permits the oxidation of Au, enabling subsequent CO adsorption. A feasible reaction pathway leading to H₂ production is identified, and it is concluded that four to six atom Au clusters at the O-vacancy sites of ceria catalyze the WGS reaction.

DOI: 10.1103/PhysRevLett.94.196102

PACS numbers: 82.65.+r, 68.35.-p, 68.43.Bc

Recent years have seen tremendous efforts directed towards the exploration of oxide-supported gold catalysts, which have been shown to exhibit exceptional catalytic ability in many important reactions [1–3]. The morphology and chemical state of the active Au species is, however, strongly disputed [1–9]. As bulk metallic Au is known to be chemically inert, it is generally believed that the specific environment of highly dispersed nanoscale Au particles in some way contributes to the catalytic activity. Indeed, the high reactivity of Au particles in CO oxidation (CO + O₂ → CO₂) was identified by a number of experimental [3,4] and theoretical studies [5,6] to derive from the properties of the Au-oxide interface. Conversely, it has also been speculated that Au ions (Au^{δ-}, Au^{δ+}) may be catalytic centers in their own right, with the oxide support playing only a relatively minor role. In line with this view, recent experiments on the water-gas-shift (WGS) reaction (CO + H₂O → CO₂ + H₂) on Au-ceria catalysts found that Au^{δ+} is the catalytically active species, while coexisting metallic Au particles (Au⁰) do not take part in the reaction [7–9]. The mechanism behind the production and activity of Au^{δ+} ions remains far from settled, however.

Evidence for the role of oxidized Au in the WGS reaction was derived from the experiments of Fu and co-workers [9]. They found that the presence of metallic Au⁰ particles in their Au-ceria catalysts does not change the catalytic performance, indicating that the neutral metals are merely spectators. Using x-ray photoelectron spectroscopy (XPS), they characterized the active species as Au cations. This remarkable finding is highly unexpected. First, Au, as one of the metals with the largest electronegativity, is normally very resistant to oxidation (Au → Au^{δ+}). Second, unlike common catalytic reactions occurring on metals (metal particles) of zero band gap, the WGS reaction seemingly occurs on entirely nonmetallic materials, i.e., Au^{δ+} and CeO₂. Instead of a high reaction barrier that would be expected due to the difficulty of electron excitation, however, the WGS reaction starts to occur at ~550 K with a low apparent reaction barrier (0.4–0.5 eV) [9]. In this work, the WGS reaction on Au-ceria was

investigated using first-principles density functional theory (DFT) calculations. We aim to answer the following fundamental questions: (i) How does Au⁰ become oxidized to Au^{δ+}? (ii) What is the size of the active site, single Au atom or small Au clusters? (iii) What is the catalytic role of the ceria support?

Undoubtedly, ceria (CeO₂) is the key to the activity of the metal-ceria catalysts. As *f*-block metal oxides, Ce_xO_y (CeO₂, Ce₂O₃) feature 4*f* orbitals of Ce in their valence states. Although ceria has long been utilized as a material for oxygen storage [10], first-principles calculations on Ce_xO_y have hitherto been prohibitive, not least because of the difficulty in describing or converging the localized *f* valence electrons [11]. Only recently have a number of DFT calculations been reported, focusing on the redox property of bulk CeO₂ and Ce₂O₃ and on surfaces of CeO₂ [11,12]. It was found in general that bulk CeO₂ and its clean surfaces can be readily reduced (Ce⁴⁺ → Ce³⁺) by removal of lattice-O atoms. So far, however, the electronic structure of metal-ceria systems remains unclear. In order to model the Au-ceria catalysts, we have chosen three typical Ce_xO_y surfaces as the model substrates, namely, the stoichiometric CeO₂{111} surface [CeO₂{111}^S, Fig. 1(a)], CeO₂{111} with surface O vacancies [CeO₂{111}^R, Figs. 1(a) and 1(b)], and fully reduced

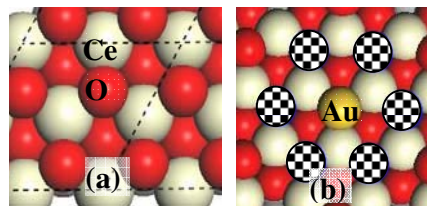


FIG. 1 (color online). Ce_xO_y surfaces modeled in our calculations. (a) Top view of CeO₂{111} surface; the Ce₂O₃{0001} surface has the similar top view as CeO₂{111} surface. (b) Top view of a Au (Au_{O-vac}) adsorption at an O vacancy of CeO₂{111}. The six surface lattice O surrounding the Au_{O-vac} are highlighted by the dotted area.

$\text{Ce}_2\text{O}_3\{0001\}$ [Fig. 1(a)]. $\text{CeO}_2\{111\}$ is chosen as the most stable (and thus dominant) surface of CeO_2 (cubic fluorite structure [12,13]); $\text{Ce}_2\text{O}_3\{0001\}$ is faceted from Ce_2O_3 [12,13] (A-type, hexagonal lattice $P\bar{3}m1$), where the nonpolar $\{0001\}$ facet is typically the most stable in hexagonal lattice materials. The existence of O vacancies in CeO_2 -based catalysts is well established in experiment and this is also confirmed in DFT calculations [12]. On going from $\text{CeO}_2\{111\}^S$ to $\text{CeO}_2\{111\}^R$ and to $\text{Ce}_2\text{O}_3\{0001\}$, the surface Ce atoms are gradually reduced from $4+$ to $3+$ (in the formal oxidation state). These model substrates therefore provide a good basis to map out the likely chemical states of the Ce_xO_y sites involved in reactions.

The $\text{CeO}_2\{111\}$ surface is modeled by a $p(2 \times 2)$ 9-layer slab (12 CeO_2 units per supercell) with the top 3 layers relaxed, and $\text{Ce}_2\text{O}_3\{0001\}$ is modeled by a $p(2 \times 2)$ 10-layer slab (8 Ce_2O_3 units per cell) with the top 5 layers relaxed. All the calculations are performed using CASTEP [14], as detailed in Ref. [15]. Our calculated lattice constants of CeO_2 ($a = 5.482 \text{ \AA}$) and Ce_2O_3 ($a = 3.897 \text{ \AA}$, $c/a = 1.58$) agree well with the experiment values (CeO_2 : $a = 5.41 \text{ \AA}$ [13]; Ce_2O_3 : $a = 3.888$, $c/a = 1.55$ [12,16]). Both oxides and clean stoichiometric surfaces are found to be insulating. CeO_2 exhibits a $2p(\text{O})$ - $4f(\text{Ce})$ band gap of 2.0 eV (expt. 3 eV), and a $2p(\text{O})$ - $5d(\text{Ce})$ band gap of 5.2 eV (expt. 6 eV), which agree generally with previous DFT calculations [12]. Underestimates in the band gaps of insulating systems are a common feature of DFT but do not affect our conclusions here. Two key issues encountered in calculating $\text{Au}/\text{Ce}_x\text{O}_y$ systems may be further addressed: (i) spin-polarized calculations are essential to describe properly the Au-ceria systems, because the presence of Au induces reduction of Ce ($\text{Ce}^{4+} \rightarrow \text{Ce}^{3+}$), leading to net spin in the Ce f states (see later discussion); and (ii) the Broyden density mixing scheme [17] meets convergence problems in magnetic systems (Ce^{3+}), apparently due to the degeneracy of the strongly localized f states. Convergence can, however, be achieved after modification of the Broyden mixing scheme by reordering and dynamically pruning the mixing history [15,18].

To investigate the most likely binding site of Au on ceria, we have first calculated the potential energy surface of a single Au atom on $\text{CeO}_2\{111\}^S$, $\text{CeO}_2\{111\}^R$, and $\text{Ce}_2\text{O}_3\{0001\}$. We found that on the $\text{CeO}_2\{111\}^S$ and $\text{Ce}_2\text{O}_3\{0001\}$ surfaces, individual Au atoms prefer to bond with the surface lattice O (labeled as $\text{Au}_{\text{latt-O}}$ hereafter), whereas on the $\text{CeO}_2\{111\}^R$ they prefer to sit in the O-vacancy site (labeled as $\text{Au}_{\text{O-vac}}$ hereafter). The adsorption energy of Au follows the order $\text{CeO}_2\{111\}^R$ (1.86 eV) $>$ $\text{CeO}_2\{111\}^S$ (1.26 eV) $>$ $\text{Ce}_2\text{O}_3\{0001\}$ (0.86 eV), which indicates that the partially reduced ceria (with O vacancies) is the best substrate to anchor Au, but that the fully reduced Ce_2O_3 is rather inert. Preferential Au adsorption at O-vacancy sites was typical for Au on oxides [19], which can be explained in terms of an enhanced ionic bonding since each O vacancy is associated with two extra electrons

left by the removed O atom. Indeed, using Bader's method [20] to analyze the DFT electron density, we found that the $\text{Au}_{\text{O-vac}}$ is strongly negatively charged ($-0.58|e|$). More surprising is that Au adatoms on the stoichiometric $\text{CeO}_2\{111\}^S$ surface are strongly *positively* charged, $+0.35|e|$ [the Bader charge of Au is typically within $\pm 0.1|e|$ in different chemical environments; for example, it is $-0.04|e|$ for a surface Au atom of $\text{Au}\{111\}$ [21], and $+0.07|e|$ for an adsorbed Au atom on stoichiometric $\text{TiO}_2(110)$ [5,19]]. This result alone confirms the unprecedented XPS observation: Au is oxidized once it is in contact with CeO_2 . It may be mentioned that the Au adatom remains largely spin polarized on $\text{Ce}_2\text{O}_3\{0001\}$ ($0.71 \mu_B$), while no net spin is found for Au on $\text{CeO}_2\{111\}^R$ and $\text{CeO}_2\{111\}^S$.

By introducing CO into these systems, we are able to probe the activity of the three $\text{Au}/\text{Ce}_x\text{O}_y$ systems towards the WGS reaction. The calculated results are summarized as follows: (i) CO only weakly adsorbs on clean oxides, both $\text{CeO}_2\{111\}^S$ and $\text{Ce}_2\text{O}_3\{0001\}$, with $E_{\text{ad}}(\text{CO}) < 0.05 \text{ eV}$; (ii) CO can attach strongly to the $\text{Au}/\text{CeO}_2\{111\}^S$ surface ($E_{\text{ad}} = 2.37 \text{ eV}$), modestly on the $\text{Au}/\text{Ce}_2\text{O}_3\{0001\}$ surface ($E_{\text{ad}} = 0.81 \text{ eV}$), but barely on the $\text{Au}/\text{CeO}_2\{111\}^R$ surface ($E_{\text{ad}} = 0.09 \text{ eV}$); and (iii) the CO-Au bonding is closely related to the oxidation state of Au (the CO-Au $^{\delta+}$ bonding is much stronger than the CO-Au $^{\delta-}$). This last fact is, perhaps, not so surprising as the bonding involving $5\sigma(\text{CO})$ donation to $6s(\text{Au})$ benefits substantially from an empty $6s(\text{Au})$ orbital [22], as in Au^+ . Indeed, in gas phase molecules the Au-CO binding energy in $[\text{Au-CO}]^+$ was determined to be $\sim 2 \text{ eV}$, much stronger than in a neutral $[\text{Au-CO}]$ molecule [23].

Having determined that individual Au atoms mainly occupy O-vacancy sites, but that the resulting $\text{Au}_{\text{O-vac}}^{\delta-}$ is inert towards CO, we rule out any catalytic mechanism based upon *only a single Au atom* or *associated with the fully reduced Ce_2O_3* . A successful catalyst clearly must bond both Au *and* CO. To consider the scenarios of more than one Au atom, we notice that, as highlighted in Fig. 1(b), each $\text{Au}_{\text{O-vac}}$ is surrounded by six surface lattice-O atoms. If subsequent Au atoms adsorb on such neighboring lattice-O atoms, perhaps they could be the potential sites for CO adsorption. Following this idea, we have calculated three configurations with 2, 3, and 4 Au atoms near an O vacancy, namely, $^n\text{Au}/\text{CeO}_2\{111\}^R$ ($n = 2, 3, 4$). In the optimized structures, the newly arrived Au atoms sit on the surface lattice O, and also bond with the $\text{Au}_{\text{O-vac}}$. After obtaining the $^n\text{Au}/\text{CeO}_2\{111\}^R$ structures, the CO adsorption in these systems has also been investigated. The calculated $E_{\text{ad}}^n(\text{Au})$ values of the n th Au atom are 2.30, 1.84, 2.45 eV for $n = 2, 3, 4$, respectively, much larger than that of Au on stoichiometric $\text{CeO}_2\{111\}^S$ of 1.26 eV [$E_{\text{ad}}^n(\text{Au}) = (E_{\text{surf}}^{n-1} + E_{\text{gas}}^1) - E_{\text{surf}}^n$, where E_{surf}^n is the total energy of the system of n Au atoms on surface; E_{gas}^1 is the total energy of a free Au atom]. That is, $\text{Au}_{\text{O-vac}}$ atoms will act as nucleation sites for the growth of small

clusters. Importantly, the additional Au atoms remain positively charged ($+0.10 \sim +0.19|e|$), and the calculated $E_{\text{ad}}(\text{CO})$ on these ${}^n\text{Au}/\text{CeO}_2\{111\}^R$ systems are 1.33, 1.38, 1.22 eV for $n = 2, 3, 4$, respectively. Our results therefore show that multiple Au atoms can adsorb in the vicinity of an O vacancy, and that the resulting monolayer Au cluster can also adsorb CO molecules on its $\text{Au}^{\delta+}$ ions.

As the presence of $\text{Au}^{\delta+}$ is the key to CO adsorption, it is essential to understand why Au can be oxidized by ceria. To this end, we have analyzed the electronic structure of the $\text{CeO}_2\{111\}^S$ surface before and after the adsorption of Au. Figure 2(a) plots the total density of states (TDOS) of $\text{CeO}_2\{111\}^S$ (top panel), which exhibits clearly a 2 eV gap between the valence band [VB, mainly $2p(\text{O})$ states] and the localized *nonbonding* $4f(\text{Ce})$ bands (*f-B*), while the conduction band minimum [CB, mainly $5d(\text{Ce})$ states] sits about 5.2 eV above the VB maximum. In addition, by calculating a system with an isolated Au atom 5 Å away from the clean surface, we found the $6s$ orbital of the Au atom lies in the middle of the $\text{CeO}_2\{111\}$ band gap. Figure 2(a) also shows the TDOS of spin α and spin β of the $\text{Au}/\text{CeO}_2\{111\}^S$ (bottom panel) separately as the system is spin polarized. It can be seen that extra states emerge between the VB and the main *f-B* due to the Au adsorption. These states are partially occupied in spin α but empty in spin β . By further plotting the spin density ($\rho_\alpha - \rho_\beta$) of the $\text{Au}/\text{CeO}_2\{111\}^S$ in Fig. 2(b), we are able to identify where the net spin resides in space. We found that the main feature of the spin density is a localized 6-lobe *f* orbital centered at a surface Ce atom, the next-nearest-neighbor of the Au atom. This *f* orbital corresponds to the *occ-f* state (occupied *f* state) in Fig. 2(a) (bottom panel). It is evident that the Au atom is oxidized by the surface Ce atom ($\text{Au} \rightarrow \text{Au}^{\delta+}$ and $\text{Ce}^{4+} \rightarrow \text{Ce}^{3+}$) even though there is no direct Ce-Au bonding. Based on these observations, the bonding picture of Au on ceria can be described as follows. As a Au atom approaches a surface lattice-O atom, its half-occupied $6s(\text{Au})$ orbital develops overlap with the low-lying fully occupied $2p(\text{O})$ states, and

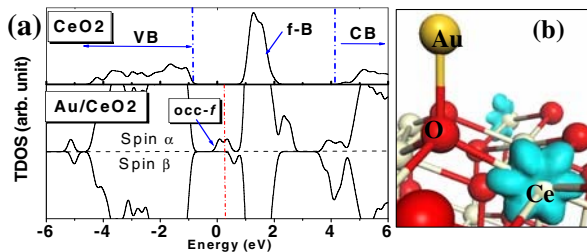


FIG. 2 (color online). (a) Total density of states of $\text{CeO}_2\{111\}^S$ (top panel) and that of $\text{Au}/\text{CeO}_2\{111\}^S$ (bottom panel). The $\text{Au}/\text{CeO}_2\{111\}^S$ system has distinct spin α and β where the plotted spin β is flipped for a clearer view. The energy zero is set to be the Fermi level of the clean $\text{CeO}_2\{111\}^S$. (b) Three-dimensional contour plot of the spin density ($\rho_\alpha - \rho_\beta$) of the $\text{Au}/\text{CeO}_2\{111\}^S$ system, showing characteristic *f*-like distribution on a single Ce ion.

evolves into the Au-O antibonding state. The antibonding electron can tunnel into the nearby empty $f(\text{Ce})$ state whenever it becomes energetically favorable for it to do so. Based on this concept, the bonding of $\text{Au}/\text{Ce}_2\text{O}_3\{0001\}$ can also be rationalized. Since the Ce in Ce_2O_3 is already reduced, the Au-O antibonding electron cannot be dumped into Ce *f* states due to the large *f-f* repulsion. Consequently, the Au adsorption energy on $\text{Ce}_2\text{O}_3\{0001\}$ is low and the net spin remains dominantly on Au, as reflected in our calculation. Therefore, the uniqueness of CeO_2 lies in the presence of empty nonbonding *f* states that sit near the Fermi level. Although rather localized, these *f* states act as an electron reservoir in accepting or donating electrons, just as the delocalized Fermi-level states do in metallic materials.

In one further step, we have investigated the possibility of the $\text{H}_2\text{O} + \text{CO} \rightarrow \text{CO}_2 + \text{H}_2$ reaction on ${}^n\text{Au}/\text{CeO}_2\{111\}^R$. On the ${}^4\text{Au}/\text{CeO}_2\{111\}^R$ surface, we have identified a feasible pathway for the WGS reaction, which follows this mechanism: $\text{H}_2\text{O} \rightarrow \text{H}_{\text{ad}} + \text{OH}_{\text{ad}}$; $\text{CO}_{\text{ad}} + \text{OH}_{\text{ad}} \rightarrow \text{CO}_2\text{H}_{\text{ad}}$; $\text{CO}_2\text{H}_{\text{ad}} \rightarrow \text{CO}_2 + \text{H}_{\text{ad}}$; $\text{H}_{\text{ad}} + \text{H}_{\text{ad}} \rightarrow \text{H}_2$. The transition states (TS) of the first three key steps were searched using the constrained-minimization technique [19,21,24] and the reaction barriers were determined. It should be mentioned that the $p(2 \times 2)$ unit cell is rather large ($7.79 \text{ \AA} \times 7.79 \text{ \AA}$) and can readily accommodate 4 Au atoms (the shortest Au-Au distance between adjacent unit cells is $\sim 4.3 \text{ \AA}$, while that in each individual cell is $\sim 2.75 \text{ \AA}$) [25]. The overall total-energy profile of this reaction is drawn in Fig. 3, together with snapshots of the clean ${}^4\text{Au}/\text{CeO}_2\{111\}^R$ surfaces and the TS structures. The pathway in Fig. 3 can be summarized as follows: (i) H_2O only weakly adsorbs on clean $\text{CeO}_2\{111\}$ and on ${}^n\text{Au}/\text{CeO}_2\{111\}^R$ surfaces with E_{ad} being 0.4–0.5 eV. This indicates that at typical catalytic conditions, e.g., 550 K, H_2O will not stick on the catalyst. Starting from the gas phase H_2O molecule, however, a modest reaction barrier of 0.59 eV is calculated for H_2O dissociation on the ${}^4\text{Au}/\text{CeO}_2\{111\}^R$ leading to adsorbed OH and H species. (ii) Once H_2O is dissociated, the OH group can react readily with CO with a barrier of only 0.10 eV. This facile reaction is exothermic by 0.37 eV. (iii) The COOH thus formed can then lose its H atom to release CO_2 , with a reaction barrier of 1.08 eV (exothermic by only 0.03 eV). (iv) At the final stage, two adsorbed H atoms recombine to form an H_2 molecule, which is endothermic by 0.90 eV. We notice that, unlike the $\text{Au}_{\text{latt-O}}$ that register with lattice-O atoms, the $\text{Au}_{\text{O-vac}}$ can have appreciable displacement during the reaction, as shown in Fig. 3, which helps to stabilize the reaction intermediates. Finally, it should be emphasized that the effect of the finite temperature and pressure (T, p) has not been taken into account in Fig. 3, where (T, p) will particularly affect the chemical potential of gas phase molecules. It is known that desorption processes, such as the $\text{H}_{\text{ad}} + \text{H}_{\text{ad}} \rightarrow \text{H}_2$ reaction, are driven by a large entropy term at elevated temperatures, so the endo-

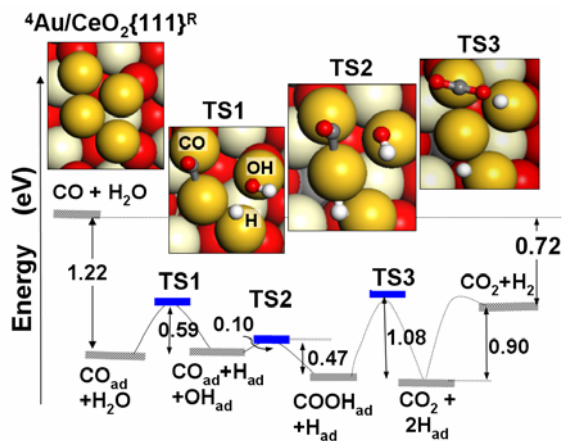


FIG. 3 (color online). The overall total-energy profile of the $\text{CO} + \text{H}_2\text{O} \rightarrow \text{CO}_2 + \text{H}_2$ reaction on a four-atom Au cluster that anchors on an O vacancy of $\text{CeO}_2\{111\}$.

thermic nature of the final step does not present a significant problem. Note also that the maximum barrier that must be overcome is 1.08 eV (TS3), so the binding energy of CO must exceed this amount if appreciable conversion is to occur. Clearly, this is true in the model considered, as a result of the positive charge state of $\text{Au}_{\text{lat-O}}$ ions in the cluster, but would not be the case if only the $\text{Au}_{\text{O-vac}}$ ion were present or if a CeO_2 support were fully reduced [8].

In summary, the present DFT calculations on the Au-ceria system provide the first theoretical framework within which the unusual nonmetallic catalysis on ceria-based catalysts may be understood. First, we have demonstrated the oxidation of Au atoms by ceria and the preferential Au adsorption and nucleation at O vacancies. Second, we showed that only $\text{Au}^{\delta+}$ can adsorb CO sufficiently strongly for subsequent catalysis, and that a combination of several such $\text{Au}^{\delta+}$ in the vicinity of an O vacancy does catalyze the WGS conversion. It is concluded that the active sites in the catalysts are neither single Au atoms nor sizeable Au particles, but ultrasmall Au clusters. The unusual catalytic ability can be attributed to the presence of empty non-bonding f states of CeO_2 that act as a particularly efficient electron buffer in reactions, just like the delocalized Fermi-level states in metals.

We acknowledge the Isaac Newton Trust (Z.-P.L.) and The Royal Society (S.J.J.) for financial support, EPSRC (UK) for computation equipment, and the UK HPCx, Cambridge-Cranfield High Performance Computing Facility for computer time.

[1] M. Haruta, *Catal Today* **36**, 153 (1997).

[2] M. Valden, X. Lai, and D. W. Goodman, *Science* **281**, 1647 (1998).

- [3] J. D. Grunwaldt, C. Kiener, C. Wogerbauer, and A. Baiker, *J. Catal.* **186**, 458 (1999).
- [4] C. T. Campbell, *Science* **306**, 234 (2004); M. S. Chen and D. W. Goodman, *Science* **306**, 252 (2004).
- [5] Z.-P. Liu *et al.*, *Phys. Rev. Lett.* **91**, 266102 (2003).
- [6] G. Mills, M. S. Gordon, and H. Metiu, *J. Chem. Phys.* **118**, 4198 (2003).
- [7] T. Bunluesin, R. J. Gorte, and G. W. Graham, *Appl. Catal. B* **15**, 107 (1998).
- [8] J. M. Zalac, V. Sokolovskii, and D. G. Loffler, *J. Catal.* **206**, 169 (2002).
- [9] Q. Fu, H. Saltsburg, and M. Flytzani-Stephanopoulos, *Science* **301**, 935 (2003).
- [10] M. S. Dresselhaus and I. L. Thomas, *Nature (London)* **414**, 332 (2001); T. Hibino *et al.*, *Science* **288**, 2031 (2000).
- [11] C. J. Pickard *et al.*, *Phys. Rev. Lett.* **85**, 5122 (2000).
- [12] N. V. Skorodumova *et al.*, *Phys. Rev. Lett.* **89**, 166601 (2002); Z. Yang, T. K. Woo, M. Baudin, and K. Hermansson, *J. Chem. Phys.* **120**, 7741 (2004).
- [13] L. Eyring, in *Handbook on the Physics and Chemistry of Rare Earths*, edited by K. A. Gschneider and L. Eyring (North-Holland, Amsterdam, 1979).
- [14] M. C. Payne *et al.*, *Rev. Mod. Phys.* **64**, 1045 (1992).
- [15] The Ce ultrasoft pseudopotential explicitly treats $5s$, $5p$, $4f$, $5d$, $6s$ as valence electrons [11]. A plane wave kinetic energy cutoff (E_{cut}) of 370 eV was used, and up to 500 eV cutoff has been used to check convergence. The grids for charge density mixing [17] and for wave-function calculation contain all wave vectors up to $2G_{\text{cut}}$ ($E_{\text{cut}} = \frac{\hbar^2}{2m} G_{\text{cut}}^2$). Such extensive grids are required in order to converge the energy of magnetic systems. The gradient-corrected exchange and correlation functional [J. P. Perdew, K. Burke, and M. Ernzerhof, *Phys. Rev. Lett.* **77**, 3865 (1996)], referred to as GGA-PBE, was used in all the calculations. The other parameters in the CASTEP calculation are the same as described in Refs. [19,21,24]. No Hubbard U term was necessary in the present work because individual f orbitals were never more than singly occupied.
- [16] R. W. G. Wyckoff and E. O. Wollan, *Acta Crystallogr.* **6**, 741 (1953).
- [17] D. D. Johnson, *Phys. Rev. B* **38**, 12 807 (1988).
- [18] Z.-P. Liu, S. J. Jenkins, and D. A. King (unpublished).
- [19] Z.-P. Liu, S. J. Jenkins, and D. A. King, *Phys. Rev. Lett.* **93**, 156102 (2004).
- [20] R. F. W. Bader, *Atoms in Molecules—A Quantum Theory* (Oxford University Press, Oxford, 1990).
- [21] Z.-P. Liu, P. Hu, and A. Alavi, *J. Am. Chem. Soc.* **124**, 7499 (2002).
- [22] P. Pykkö, *Angew. Chem., Int. Ed.* **43**, 4412 (2004).
- [23] See, e.g., T. K. Dargel, R. H. Hertwig, W. Koch, and H. Horn, *J. Chem. Phys.* **108**, 3876 (1998), and references therein.
- [24] Z.-P. Liu, S. J. Jenkins, and D. A. King, *J. Am. Chem. Soc.* **126**, 10 746 (2004).
- [25] This is also consistent with the fact that the structure of the four-Au atom cluster from the $p(2 \times 2)$ cell calculation is well maintained in a $p(3 \times 3)$ cell calculation.